Atomic and electronic structure of the (4×1) and (8×2) In/Si(111) surfaces

Shiow-Fon Tsay*
Department of Physics, National Sun Yat-sen University, Kaohsiung, Taiwan 804, Republic of China
(Received 26 September 2003; revised manuscript received 1 September 2004; published 13 January 2005)

The atomic and electronic structures of the (4×1), (4×2), and (8×2) phases of In on a Si(111) surface were investigated using the local-density approximation of the density-functional theory. The pairing of the outer In adatoms in the zigzag chains reduces the system's total energy and doubles the periodicity in the $\vec{b}$ direction. The opposite displacements of the neighboring Si zigzag chains generate a glide-plane symmetry. As the surface structure changes from (4×1) to (8×2), atomic reconstruction yields double lattice periodicity, charge density modulation, band splitting, and the opening of pseudogaps and lowers the system's total energy. It also changes the electrical characteristics from being metallic to imperfectly insulating, with small pseudogaps, 31 and 153 meV, at the surface Brillouin zone boundary points $\bar{X}_2$ and $\bar{Y}$, respectively. Hence, we believe that the transition between the (4×1) and the (8×2) phase on the Si(111) surface is driven by a quasi-one-dimensional charge-density wave. The interchain interaction between the In chains plays an important role in stabilizing the CDW of the (8×2) phase. The calculated atomic and electronic structures of these phases are consistent with the results of surface x-ray diffraction and angle-resolved photoemission spectroscopy, respectively.

DOI: 10.1103/PhysRevB.71.035207 PACS number(s): 68.35.Bs, 68.35.Rh

Adsorption of In on Si(111) leads to various surface reconstructions that are semiconducting at coverages below a single monolayer (ML) but metallic at higher coverages. Lander and Morrison observed a (4×1) phase at the border of these two regions (~1 ML).[1] The atomic and electronic structures of the (4×1) phase of In on a Si(111) surface have been studied both theoretically and experimentally.[1–10] The surface structure of the (4×1) phase was determined only recently by means of surface x-ray diffraction (SXRD).[2] The observed surface structure consists of zigzag quasi-one-dimensional In chains in the $[\bar{1}10]$ direction, separated by parallel Si-adatom chains.[2] Kraft *et al.*[3] used scanning tunneling microscopy (STM) and scanning tunneling spectroscopy (STS) techniques to demonstrate that the (4×1) phase is semimetallic. Abukawa *et al.*[7] applied angle-resolved photoemission spectroscopy (ARPES) to establish that the (4×1) phase of In on a Si(111) surface is metallic. They found three surface-state bands cross the Fermi level E_F in the $\bar{\Gamma}\bar{X}_1$ direction (parallel to the In chains) and that the no surface-state band crosses E_F in the $\bar{\Gamma}\bar{X}_1'$ direction (perpendicular to the In chains). Independent ARPES (Ref. 8) and inverse photoemission spectroscopy[9] (IPES) also have verified the anisotropic dispersion and metallic behavior of the (4×1)-In/Si(111) surface. Recently, Yeom *et al.*[8] combined ARPES and STM measurements and reported that an In/Si(111) system undergoes a reversible phase transition from its (4×1) structure at room temperature (RT) to semiconducting (4×"2") or (8×"2") structure at around 100 K, driven by a one-dimensional (1D) charge-density wave (CDW) or, equivalently, Peierls instability along the In chain. The term ×"2" means an incomplete long-range order of the double periodicity across the one-dimensional chains, so that only half-order streaks appear in diffraction patterns instead of half-order spots.[8,11]

Photoemission spectroscopy shows that pseudogaps seem to open up in the surface band structure of the 8×"2" phase at low temperatures (LT).[12] Assuming the gap is symmetric relative to the Fermi level, the size of the gaps are estimated to be 150±40 and 80±10 meV. However, Sakamoto *et al.*,[13] applying high-resolution electron-energy-loss spectroscopy (HREELS) determined that the (8×2) phase was not purely semiconducting at 90 K. In explaining the inconsistency between the electronic characteristics of the (8×"2") phase determined by the HREELS (Ref. 13) and ARPES (Ref. 8 and 12) studies, Sakamoto *et al.* posited that either CDW is completely absent or the (8×"2") phase is partly metallic due to the instability of the 1D CDW because of the significant reduction of surface free carrier density.[13] On the other hand, the SXRD measurements made by Kumpf *et al.* at 20 K revealed that the LT phase was an (8×2) reconstruction, primarily due to the formation of In trimers within the In chains.[14] They also found very strong chain-to-chain correlations, but only in the direction perpendicular to the chain, and concluded that the phase change was not driven by CDW.

Theoretical work on the atomic and electronic structure of the In/Si(111) system have been limited to the (4×1) phase.[15–17] The only calculation[15] related to the (8×2) phase yields results inconsistent with the SXRD data[14] and suggests no opening of the band gap at the Fermi level, thus contradicting the original experimental claim.[8,12] Therefore, the surface reconstruction and the electronic structures of In adsorbed on Si(111) surface with 1 ML of In coverage warrant investigation. This present study performed calculations from first principles, based on the density-functional theory (DFT). The atomic and electronic structures of the (4×1), (4×2), and (8×2) phase are presented. On the (4×1) phase, more accurate atomic and electronic structural results than the previous study[15–17] are reported. On the (8×2) phase, our calculated atomic structure agrees with the SXRD data of Kumpf *et al.*,[14] and the electronic structure explains

the ARPES results undertaken by Abukawa *et al.*[7] and Yeom *et al.*,[8,12] and the HREELS data obtained by Sakamoto *et al.*[13]

The calculations were made using VASP[18–20] (Vienna *ab initio* simulation package) developed at the Institut für Material Physik of the Universität Wien. The calculations of total energy from first principles were performed using the local-density approximation (LDA) of DFT. The Ceperley-Alder[21] exchange-correlation function, as parametrized by Perdew and Zunger, was adopted.[22] A repeated-slab supercell model was used. Each slab included ten atomic layers of Si and an adlayer of Si and In, H atoms were attached to the bottom layer of Si atoms to saturate the Si's dangling bonds. The width of the vacuum region between adjacent slabs was set to be about 10.0 Å, which is large enough to prevent coupling between slabs. The same (8×2) unit cell was considered for the (4×1)-, (4×2)-, and (8×2)-In/Si(111) surfaces, enabling their total energies to be compared. The pseudopotentials of the electron-ion, supported by VASP were specified using the projector-augmented wave (PAW) method.[23] The 4*d* electrons of In were regarded as valence electrons in the PAW potential. The wave functions were expanded using a plane-wave basis set with an energy cutoff of 22.97 Ry. A (2×8) Monkhorst and Pack[24] mesh, equivalent to eight irreducible **k** points was used to sample the surface Brillouin zone of the (8×2) unit cell during the atomic structural relaxation. The Davidson-block algorithm was applied to optimize the energy of the electronic state to meet a 1×10^{-6} eV stopping criterion. Additionally, a conjugate gradient algorithm was implemented to relax the atomic positions until the total energy changed by less than 1 meV per (8×2) cell, such that the atomic force acting on each ion was under 0.02 eV/Å.

The (8×2) unit cell comprises two (4×2) subcells, each of which contains four Si adatoms and four inner In adatoms (3–6) at the on-top sites; two outer In adatoms In(1) and In(2) at the H_3 sites and In(7) and In(8) at the T_4 sites as shown in Fig. 1. The initial vertical positions of all Si and In adatoms are the same. Figure 1 displays the top and side views of the optimal atomic structure, and Table I lists the optimized atomic positions of the (4×1)-In/Si(111) phase. In Table I, the coordinates are measured in unit of basic vectors $\vec{a}=(a_0/2)[10\bar{1}]_{\text{substrate}}$, $\vec{b}=(a_0/2)[\bar{1}10]_{\text{substrate}}$, and $\vec{c}=(a_0/3)[111]_{\text{substrate}}$, where a_0 is the calculated bulk lattice constant 5.402 Å (including a 0.5% error from the experimentally determined value). For comparison, Table I also lists the SXRD results obtained by Bunk *et al.*[2] and the ideal bulklike positions. It reveals that the optimal positions of In(1), In(3), In(5), and In(7) are not exactly at H_3, the on-top, and the T_4 sites, respectively. The deviations from the positions determined by SXRD are less than 0.17 Å. The results are consistent with other theoretical results based on DFT.[25] A large energy cutoff 33.09 Ry for the plane-wave basis set was also applied. The differences between the optimal atomic positions calculated with different energy cutoffs are below 0.01 Å. In fact, the discrepancy between the theoretical and experimental atomic positions is in the same order of magnitude as the simulation was performed in another computational approach.[26] That approach was based on DFT and the norm-conserving pseudopotential with localized basis sets and the Bloch sums of *s*, p_x, p_y, and p_z orbitals. Consequently it can be concluded that the deviation is not caused by the low-energy cutoff. However, it must be noted that the atomic coordinates determined by different experiments may result in significant deviations. The LEED analysis is more sensitive to perpendicular distortions in outermost layers, while the SXRD measurement is more sensitive to parallel distortions in deep layers. Hence, the simulation results presented agree closely with the experimental values obtained by SXRD measurements.[2]

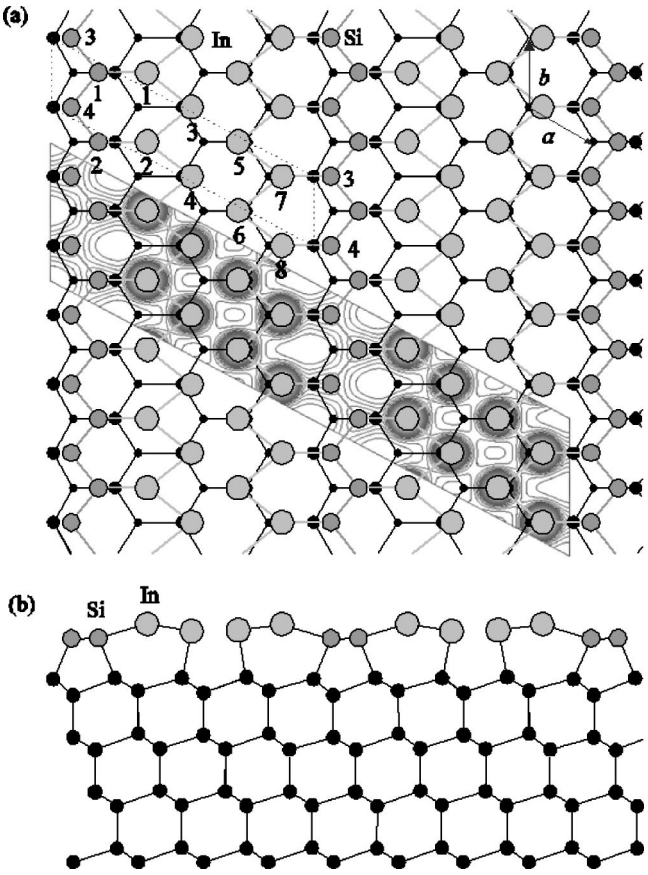

FIG. 1. Top (a) and side (b) views of the optimized geometry of (4×1)-In/Si(111). Dashed lines refer to the (4×1) unit cell. In and Si adatoms are plotted as large filled and middle-size filled circles, respectively. In the top view, small black filled circles represent Si atoms in the first and second layers of the substrate. Total valence charge density map on the (111) plane cut by the topmost In atom, In(7), also shown in (a).

Table II presents the interatomic distances of the (4×1) surface structure. The In(1)-Si(1) and In(7)-Si(3) distances are 2.62 and 2.61 Å, respectively, and they are both similar to the sum of the covalent radii of Si and In, 2.56 Å (=1.11 Å+1.44 Å),[27] indicating that the Si atoms and the neighboring In atoms are covalently bonded. The total valence charge-density on the (111) plane cut by the topmost In atom, In(7), as shown in Fig. 1, indicates that a significant amount of the valence charges between In(1) and Si(1) are consistent with the formation of a bond between them. The same occurs to the bond between In(7) and Si(3). However,

TABLE I. Calculated positions of atoms in the (4×1)-In/Si(111) system. Columns 2 and 3 present the ideal (bulklike) and experimentally determined (Ref. 2) atomic positions, respectively, for comparison. Column 5 presents differences between the experimental and calculated atomic positions.

	Ideal bulklike	Bunk *et al.*	This work	d(Å)
In		(0.11, 0.06, 0.86)	(0.144, 0.07, 0.831)	0.14
In		(0.86, 0.93, 0.85)	(0.870, 0.935, 0.845)	0.03
In		(1.53, 0.77, 0.99)	(1.540, 0.770, 0.953)	0.12
In		(3.43, 0.22, 0.99)	(3.473, 0.236, 0.960)	0.17
Si		(2.28, 0.14, 0.73)	(2.294, 0.147, 0.702)	0.09
Si		(2.71, 0.86, 0.76)	(2.713, 0.857, 0.720)	0.13
Si	(1.000, 1.000, 0.000)	(0.96, 0.98, 0.04)	(0.992, 0.996, 0.012)	0.14
Si	(2.000, 0.000, 0.000)	(2.01, 0.00, −0.03)	(2.025, 0.012, −0.018)	0.06
Si	(3.000, 1.000, 0.000)	(2.95, 0.97, −0.01)	(2.973, 0.986, 0.012)	0.09
Si	(4.000, 1.000, 0.000)	(3.96, 0.98, −0.00)	(4.025, 1.012, −0.003)	0.16
Si	(0.333, 0.667, −0.250)	(0.31, 0.65, −0.26)	(0.334, 0.667, −0.267)	0.08
Si	(1.333, 0.667, −0.250)	(1.30, 0.65, −0.25)	(1.335, 0.667, −0.224)	0.14
Si	(2.333, 0.667, −0.250)	(2.29, 0.64, −0.33)	(2.330, 0.665, −0.304)	0.15
Si	(3.333, 0.667, −0.250)	(3.29, 0.65, −0.23)	(3.328, 0.664, −0.222)	0.13
Si	(0.333, 0.667, −1.000)	(0.33, 0.67, −1.01)	(0.333, 0.667, −1.012)	0.02
Si	(1.333, 0.667, −1.000)	(1.32, 0.66, −0.99)	(1.337, 0.669, −0.984)	0.06
Si	(2.333, 0.667, −1.000)	(2.32, 0.66, −1.04)	(2.331, 0.666, −1.043)	0.04
Si	(3.333, 0.667, −1.000)	(3.31, 0.65, −0.98)	(3.330, 0.665, −0.982)	0.07
Si	(0.667, 0.333, −1.250)	(0.66, 0.33, −1.24)	(0.672, 0.336, −1.251)	0.05
Si	(1.667, 0.333, −1.250)	(1.65, 0.32, −1.26)	(1.657, 0.328, −1.256)	0.03
Si	(2.667, 0.333, −1.250)	(2.67, 0.33, −1.27)	(2.675, 0.337, −1.267)	0.03
Si	(3.667, 0.333, −1.250)	(3.66, 0.33, −1.25)	(3.662, 0.331, −1.243)	0.02

the interatomic distances of In(1)-In(3) and In(2)-In(3), 2.96 Å, are much shorter than those of In(1)-In(2) and In(3)-In(4), 3.82 Å. In(2), In(4), In(6), and In(8) exhibit the same relationship as presented in Table I. The interatomic distance of In(3)-In(5), 3.07 Å, also exceeds that between In(3) and the Si substrate, 2.64 Å. These facts imply that two zigzag-In chains are formed in each (4×1) unit cell as presented in Fig. 1. The heights of the In adatoms are different—$\Delta h_{\mathrm{In(1)\text{-}In(3)}}=0.40$ Å and $\Delta h_{\mathrm{In(7)\text{-}In(5)}}=0.33$ Å—so these two zigzag In chains are not equivalent, since the In(1) and In(7) adatoms have different environments. The nearest-neighbor distances (NND's) of In atoms are within the range 2.94–3.07 Å. Such results are consistent with the experimental values, since the bond lengths between the In atoms are in the range 2.98–3.14 Å. However, the NND among the In atoms given by Cho *et al.*,[15] Nakamura *et al.*,[16] and Miwa *et al.*[17] are in the range of 3.04–3.12 Å, 3.01–3.07 Å, and 2.89–3.09 Å, respectively. The variation among the theoretical results is attributable to the use of different pseudopotentials and optimized lattice constants (5.40–5.47 Å) of Si bulk.

Going beyond the (4×1) structure, the In adatoms were pushed slightly away from their optimal (4×1) positions and then structural relaxation simulations were performed. All atoms were relaxed until the total energy changed by under 10^{-3} eV per (8×2) unit cell. Two distinct phases of In/Si(111) are obtained here. The (8×2) structure has a total energy of 17.0 meV per (8×2) unit cell less than that of the (4×1) structure.[28] The (4×2) structure is more stable than the (4×1) structure by 4.0 meV per (8×2) unit cell. The structures (4×1) and (4×2) have almost degenerated and the (8×2) phase is more stable than the other two phases. Other different structures may be possible, structures that we did not present here because of the limitation of our computing resource. However, the presented phases are consistent with recently obtained experimental results,[11,14] and also show that various phases coexist during the phase transition.[11]

Table II also presents the relative interatomic distances of the above two phases. In the first and the second blocks of Table II, the relative covalent bond lengths In-In, Si-Si, and In-Si show no significant difference between the (4×2) and the (4×1) phases. Indeed, the surface structure of the (4×2) surface phase does not differ markedly from that of the (4×1) surface phase except in that (1) the distances between the outer In adatoms In(1)-In(2) and In(7)-In(8) are slightly shorter ($\sim$0.06 Å) in the former, indicating that the outer In adatoms tend to pair in the (4×2) phase and (2) the distances between the two zigzag indium chains in the (4×2) phase are also slightly shorter than in the (4×1) phase. Hence, the surface structure of the (4×2) phase exhibits a double periodicity modulation along the indium chains and the surface lattice distortion reduces the total system's en-

TABLE II. Calculated atomic distances (in unit Å) between In and Si adatoms and substrate atoms in the (4×1), (4×2), and (8×2) phases. The atoms are labeled as described in Figs. 1 and 2.

	(4×1)-In/Si(111)	(4×2)-In/Si(111)	(8×2)-In/Si(111)
In(1)—Si(1)	2.62	2.62	2.62
In(2)—Si(2)	2.62	2.63	2.59
In(7)—Si(3)	2.61	2.62	2.58
In(8)—Si(4)	2.61	2.62	2.63
In(1)—In(3)	2.96	2.96	2.99
In(2)—In(4)	2.96	2.98	2.91
In(1)—In(4)	2.96	2.96	2.86
In(2)—In(3)	2.96	2.97	2.94
In(5)—In(7)	2.94	2.96	2.90
In(6)—In(8)	2.94	2.98	2.99
In(5)—In(8)	2.94	2.96	2.87
In(6)—In(7)	2.94	2.96	2.90
In(3)—In(5)	3.07	3.04	2.90
In(4)—In(6)	3.07	3.08	2.90
In(3)—In(6)	3.07	3.02	3.58
In(4)—In(5)	3.07	3.01	4.38
In(1)—In(2)	3.82	3.76	3.19
In(3)—In(4)	3.82	3.79	3.71
In(5)—In(6)	3.82	3.79	3.76
In(7)—In(8)	3.82	3.74	3.14
Si(1)—Si_{sub}	2.39	2.39	2.37
Si(1)—Si(3′)	2.36	2.36	2.35
Si(1)—Si(4′)	2.36	2.36	2.37
Si(2)—Si(4′)	2.36	2.36	2.36
Si(2)—Si(3′)	2.36	2.36	2.35
In(3)—Si_{sub}	2.64	2.65	2.68
In(4)—Si_{sub}	2.64	2.64	2.62

ergy. Cho *et al.* have also theoretically reproduced this phase.[15]

Figure 2 reveals the other phase, displaying top and side views of the optimal atomic structure of the (8×2) phase. The (8×2) unit cell, defined by black dashed lines in Fig. 2, includes two (4×2) subcells indicated by dotted lines; one contains In adatoms 1–8 and the other contains In adatoms $1'-8'$. The (8×2) configuration can be regarded as two (4×2) subcells related by a glide plane (indicated by a dot-dashed line). The open circles in Fig. 2 represent the In and Si adatoms in the (4×1) structure. Comparing Fig. 2 with Fig. 2 of Ref. 14 reveals that the atomic displacements of the (8×2) structure, relative to the (4×1) structure, are highly consistent with the model of the LT (8×2)-In/Si(111) reconstruction.[14] No other theoretical researchers have reproduced this phase so far.[12] Kumpf *et al.*[14] also argued that the periodicity of the (8×2)-In/Si(111) along the indium chains is doubled by the pairing of the outer indium chains, resulting in the formation of indium trimers whose interatomic distances are between 2.8 and 3.1 Å. Even though we obtained similar interatomic distances (between 2.86 and 3.19 Å as listed in Table II) which agree with experiment, the formation of trimers is not evident from our calculation in terms of interatomic distances or the valence charge distribution (Fig. 3). The substrate atoms of the (8×2) phase are basically not displaced from those in the (4×1) phase, except in the first and second layer of the substrate Si atoms under In(1) and In(3), which exhibit small displacements $\sim$0.11 Å, which are less than those noted by Kumpf *et al.* $\sim$0.4 Å.[14]

The way we see the surface phase transition is as follows. Pairing of the outer indium adatoms In(1)-In(2) and In(7)-In(8) reduces the total energy of the system when the (4×1) phase is transformed into the (4×2) phase. This suggests that the pairing will persist when the surface structure transition $(4\times2)\rightarrow(8\times2)$ occurs. In order to maintain the covalent bond lengths of Si-In and Si-Si, the Si adatoms next to the zigzag In chains are substantially displaced in the $\vec{b}$ direction and in opposite direction in the neighboring Si rows as shown in Fig. 2. This tiny change was observed experimentally as depicted in Fig. 2 of Ref. 14. This effect strengthens the pairing of the outer In adatoms, thereby reducing the interatomic distances between In(1) and In(2), and between In(7) and In(8) from 3.83 Å in the (4×1) struc-

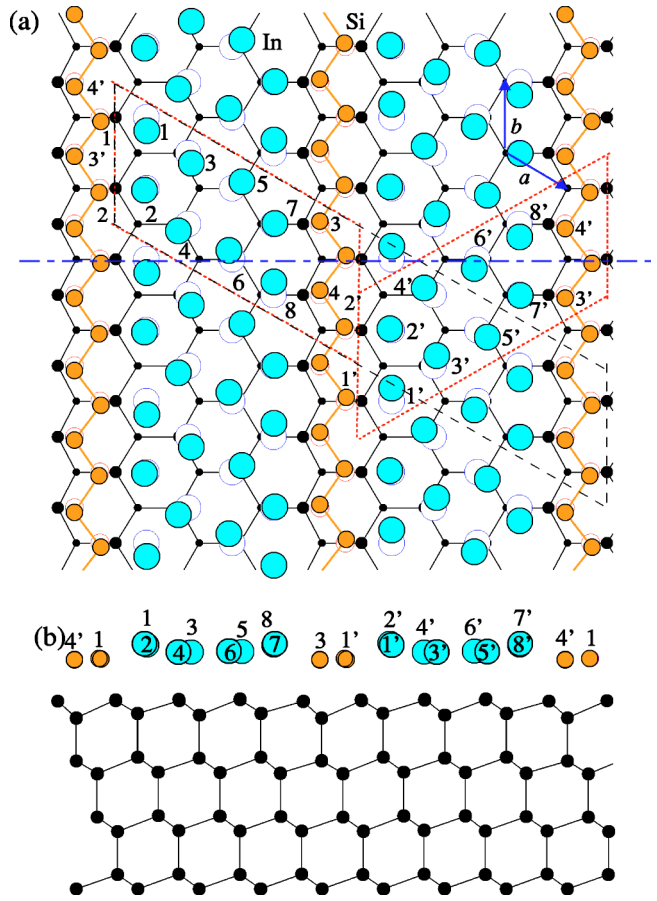

FIG. 2. Top (a) and side (b) views of the optimized geometry of (8×2)-In/Si(111). Dashed lines refer to the (8×2) unit cell. Large filled and middle-size filled circles represent the In and Si adatoms, respectively. In the top view, small black filled circles represent Si atoms in the first and second layers of the substrate. For comparison, open circles represent the positions of the In and Si adatoms on the (4×1) structure surface. The dot-dashed line represents the glide plane.

ture to 3.19 and 3.14 Å, respectively, in the (8×2) structure. The outer In adatoms also drag inner In adatoms [In(3)–In(6)]. Therefore, within each (4×2) subcell, the inner adatoms In(3) and In(6) move toward the center of the In chains, but In(4) and In(5) move away from it. These atoms are displaced not only parallel to the chain but perpendicular as well. Finally, In adatoms In(2), In(7), In(2′), and In(7′) are only displaced slightly (<0.15 Å), whereas the other In adatoms are displaced markedly ($\geqslant0.60$ Å). In conclusion, the formation of the In pairs doubles the periodicity of the In chains in the $\vec{b}$ direction. The opposite displacements of the neighboring Si zigzag chains generate the glide symmetry. The presented atomic reconstruction process of phase transition is similar to one of the two scenarios of phase transition as suggested by Mizuno *et al.*[10]

For the (8×2) phase, the interchain distances in both In(3)-In(5) and In(4)-In(6), 2.90 Å, are shorter than the corresponding distances in the (4×1) structure, 3.07 Å and is close to the indium covalent bond length of 2.88 Å.[27] This indicates that the inter-In-chain interaction is significant in

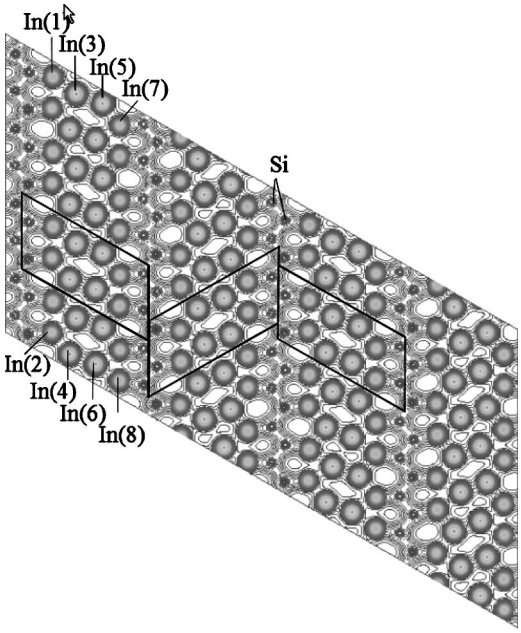

FIG. 3. Total valence charge density map of (8×2)-In/Si(111) on the (111) plane cut by the topmost In atom.

the (8×2) structure and that the quasi-one-dimensional characteristic of the In chains in the (4×1) phase will be suppressed. This fact is evidenced by the contrast between the total valence charge density distribution in the (8×2) phase, as depicted in Fig. 3, with that of the (4×1) phase, as depicted in Fig. 1. Some charge density exists in the regions between In(3) and In(5) and between In(4) and In(6) of the (8×2) phase, whereas the charge density over those regions of the (4×1) phases is significantly smaller. The difference of the valence charge density distributions between the inner In rows of both phases is related to the change of the filled-state STM images when a phase transition from the 4×1 to the 8×2 phases occurs (as shown in Fig. 1 of Ref. 11). Experiments show that each (4×1) stripe (as a 4×1 unit cell shown by the dotted lines in Fig. 1, or as shown in Fig. 1 of Ref. 11) of the STM image can be divided into two subchains in the (4×1) phase. When the complete $8\times$"2" phase is formed, the STM image shows that the stripe becomes a "$\times2$" periodicity (as a 4×2 unit cell shown by the solid lines in Fig. 3) consisting of elongated protrusions connecting between the subchains in each stripe. The neighbor elongated protrusions having different inclinations show an "$\times8$" periodicity. It is worth noting how the neighboring stripes are shifted along the chain, as shown in Fig. 1(d) of Ref. 11. These characteristics of both phases are clearly evident in our calculated valence charge density distributions as shown in Figs. 1 and 3. Hence, we believe that our calculated (8×2) structure is close to the experimental observed $(8\times$"2") structure.[11,14] Figure 3 also shows the valence charge density on the inner In rows is larger than that on the outer In rows. Such well confined valence charge density may be related to the LT STM image showing a rather sharp charge-density on the central part of the elongated protrusions. Hence, we postulate that the interchain interactions are significant in the (8×2) phase, and the structural phase tran-

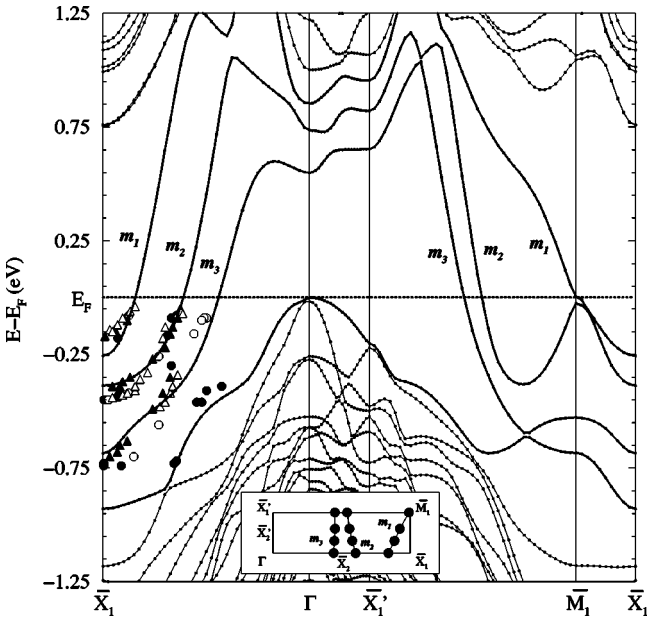

FIG. 4. Electronic surface band structures of (4×1)-In/Si(111). The labels m_1, m_2, and m_3 are the same as used by Abukaka *et al.* (Ref. 7). Full circles, empty circles, full triangles, and empty triangles represent the ARPES data of Yeom *et al.* (Fig. 3 of Ref. 12) along the first $(\bar{\Gamma}_1-\bar{X}_1)$, the first $(\bar{X}_1-1.5\bar{X}_1)$, the third $(\bar{\Gamma}_3-\bar{X}_3)$, and the third $(\bar{X}_3-1.5\bar{X}_3)$ surface Brillouin zone lines, respectively, as plotted using the reduced zone scheme. The inset shows the two-dimensional Fermi surfaces for three surface bands.

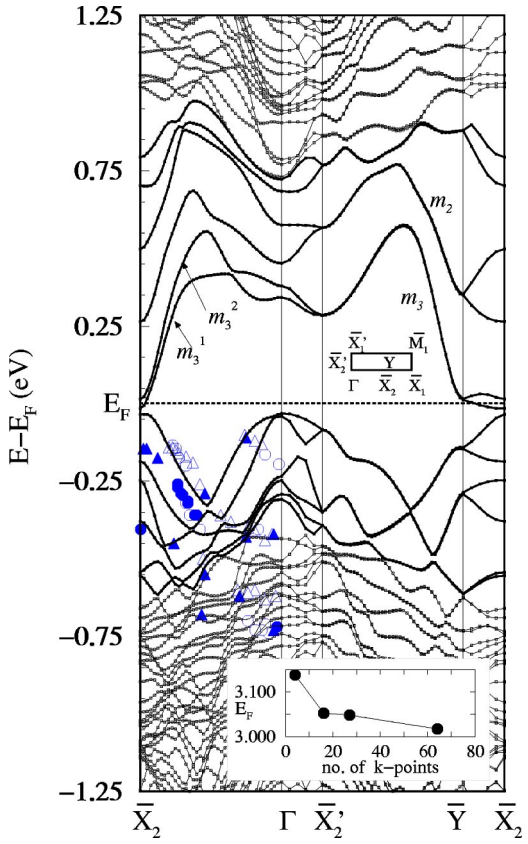

FIG. 5. Electronic surface band structures of (8×2)-In/Si(111). The special points of the surface Brillouin zone for the (4×1) and (8×2) unit cells are shown also. Full circles, empty circles, full triangles and empty triangles represent the ARPES data of Yeom *et al.* (Fig. 3 of Ref. 12) along the first $(\bar{\Gamma}_1-\bar{X}_1)$, the first $(\bar{X}_1-1.5\bar{X}_1)$, the third $(\bar{\Gamma}_3-\bar{X}_3)$, and the third $(\bar{X}_3-1.5\bar{X}_3)$ surface Brillouin zone lines, respectively, as drawn in reduced zone scheme. The inset displays the relation between the calculated Fermi energy with the number of k points.

sition is responsible for modulating the valence charge density.

Figures 4 and 5 display the surface electronic band structures of the (4×1)- and (8×2)-In/Si(111), respectively. A rectangular (4×1) surface Brillouin zone is considered,[7] in which the $\overline{\Gamma X_1}$ and the $\overline{\Gamma X_1'}$ directions are parallel and perpendicular to the atomic chains, respectively. The Fermi levels plotted in Figs. 4–7 are determined by using the (4×16) Monkhorst and Pack[24] mesh, representing 32 irreducible **k** points in the surface Brillouin zone of an (8×2) unit cell. Figure 4 shows that the surface electronic band structure in the (4×1) phases is highly consistent with the results obtained by the ARPES,[12] which are also depicted in the figure using the reduced zone scheme. In Fig. 4, three metallic surface states m_1, m_2, and m_3 cross the Fermi level at 0.84, 0.60, and 0.44 $\overline{\Gamma X_1}$ lengths, and at 0.99, 0.54, and 0.45 $\overline{X_1'M_1}$ lengths, respectively. The values are consistent with the experimental results[7,8] 0.86, 0.60, and 0.44 $\overline{\Gamma X_1}$ lengths and 1.00, 0.60, and 0.48 $\overline{X_1'M_1}$ lengths, respectively. The calculated Fermi surfaces of these three surface states are shown in the inset of Fig. 4. They are in excellent agreement with ARPES results that obtained by Abukawa *et al.*[7] and the other theoretical results as calculated by Nakamura *et al.*[16] It must be noted that the m_3 band displays a quasi-one-dimensional metallic character along the In chains because the dispersion of the m_3 band is approximately straight along the $(4\times)$ direction, as shown in the inset of Fig. 4. From the analysis of the *spd* orbital and site projected character of each band, the three metallic surface states are attributable to the metallic In-5*p* orbitals (as suggested by Abukawa *et al.*[7]) and to the Si-3*p* orbitals of the substrate Si atom (as suggested by Nakamura *et al.*[15]). Near the Fermi level, the states are mainly attributable to the inner In atoms In(3) and In(5). The states which below the Fermi level near the surface Brillouin zone boundary and the surface band minimum are mainly attributed not only to covalentlike bondings between In atoms and substrate Si atoms beneath In(3) and In(5), In(3)-Si_{sub}, and In(5)-Si_{sub}, but also to covalentlike bondings between In atoms and surface Si atoms In(1)-Si(1) and In(7)-Si(3). It is also indicated by our calculated partial density of states of surface adatoms as shown in Fig. 6. No surface states cross the Fermi level along $\overline{\Gamma X_1'}$ or $\overline{M_1X_1}$, which are both perpendicular to the In chains. A finite-energy gap was observed along $\overline{\Gamma X_1'}$, indicating that the (4×1) surface seems to be semiconducting perpendicular to the In chains. The anisotropy associated with the relevant electronic states presented in Fig. 4 also has been confirmed experimentally.[7]

As the surface structure changes from the (4×1) to the (8×2) phase, the doubled periodicity of the surface In atoms

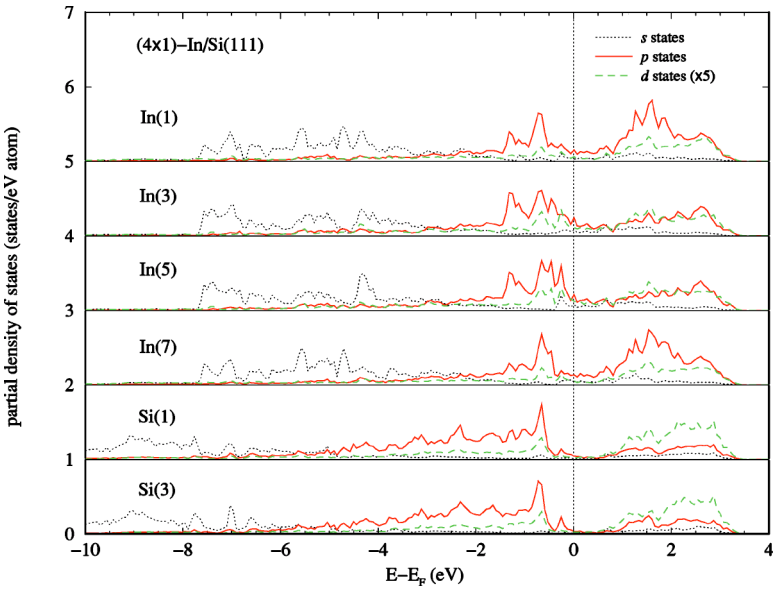

FIG. 6. Partial charge densities of states of In and Si adatoms of (4×1)-In/Si(111). The atoms are labeled as in Fig. 1 and Table I. The partial densities of *s*, *p*, and *d* states are plotted as dotted, solid, and dashed curves, respectively. The partial densities of *d* states have been multiplied by 5.

along the chain reduces the periodicity of the band structures of In in the $\overline{\Gamma X_1}$ and $\overline{X_1 M_1}$ directions. Comparing Figs. 5 with 4, it shows that each doubly degenerated surface band of the (4×1) phase is split into two bands except along the $\overline{YX_2'}$ line. For example, the m_3 band is split into $m_3{}^1$ and $m_3{}^2$ as indicated in Fig. 5. Near $\overline{X_2}$ $(=0.5\overline{X_1})$, where the m_3 band crosses the Fermi level in the (4×1) structure, the conduction bands of In interact with the valence bands of Si. Conduction-valence band mixing causes anticrossing between the conduction bands of In and the valence bands of Si, creating a pseudogap, as shown in Fig. 5. The same effect also occurs along the $\overline{YX_2'}$ line. Near the Fermi level are two pseudogaps—one at $\overline{X_2}$, and the other at $\overline{Y}$; the gap widths are 31 and 153 meV, respectively. This finding is consistent with recently obtained high-resolution photoemission data,[12] but exhibits some differences from the experimentally assessed sizes of the gaps, 80 ± 10 and 150 ± 40 meV. The differences may be caused by the assumption of the symmetric

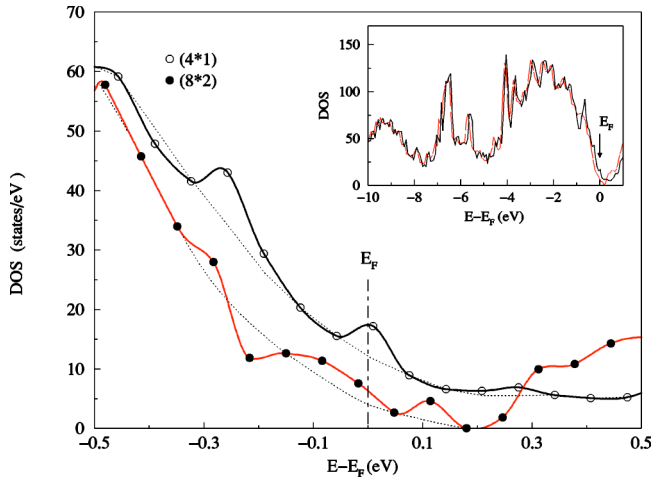

FIG. 7. Total density of states (DOS) near the Fermi level of the (4×1) and the (8×2) phases within an (8×2) unit cell. The inset displays the same DOS but with a wide energy range.

gap when the size of the gaps was estimated experimentally[12] or by the theoretical limitation of the LDA calculation on the band gap problem.[29] The fact that LDA calculations tend to underestimate band gaps is well known and is consistent with the experimental results herein. It must be noted that the calculated Fermi level in this work is determined using the 4×16 Monkhorst and Pack mesh (32 irreducible **k** points) in the surface Brillouin zone of an (8×2) unit cell, under the limitation of the computational resource. In fact, we can infer that our calculated Fermi level is overestimated according to the convergent tendency of the Fermi energy with respect to the number of **k** points (see the inset of Fig. 5). The overestimated value of the Fermi level is less than 10 meV which is the same order of magnitude of energy difference between the conduction band minimum and the Fermi level (~6 meV). Hence, we postulate the Fermi level will skim over the minimum of the conduction band at $\overline{X_2}$ point. Accordingly, we believe that a pseudogap is opened up at $\overline{X_2}$. Figure 5 also reveals that the ARPES (Ref. 12) data in the reduced zone scheme are consistent with the calculated band structures. It is worth noting that the calculated band structure will shift to higher energy and should be more consistent with the results of ARPES if the Fermi level is lowered as postulated.

Comparing Fig. 5 with the inset of Fig. 4 about near Fermi level in the $\overline{YX_2}$ direction (perpendicular to the In chains), it is noted that the dispersion of the m_3 band of the (8×2) phase is no longer as flat as that of the (4×1) phase. Therefore, the quasi-one-dimensional behavior disappears when the (4×1) structure is transformed into the (8×2) structure as before, in terms of interatomic distances and valence charge density distribution. The densities of states (DOS) of both phases are shown in Fig. 7. It is evident that the DOS of the (8×2) phase is roughly half that of the (4×1) phase near the Fermi level. This result explains why the remaining intensity of LT ARPES (Ref. 12) at Fermi level is observed, which roughly half of that at RT, and why the intensity of the Drude tail of the HREELS spectra[13] at 70 K becomes much smaller than that at RT but

still observable. The pseudogap appears as a result of the fluctuations between the metallic and insulating states and leads to a strong reduction of the spectral intensity near the Fermi level.[12] The declining surface free carrier density near the Fermi level and the opening of a small pseudogap cause the (8×2) phase to behave as an imperfect electrical insulator, as stated in Refs. 12 and 13.

The partial densities of states of the surface atoms for the (4×1) structure as plotted in Fig. 6 show that (1) the Si chains are almost semiconducting because they have an energy gap and because the charge densities of states of the Si adatom are almost zero at the Fermi level, (2) most of the conducting electrons in the In atoms are 5*p* electrons and only a few are *s* electrons, and (3) near the Fermi level, the charge densities of the 5*p* state of the inner In atoms, In(3) and In(5) exceed those of the outer In atoms, In(1) and In(7) so that the inner In rows in each chain have a higher metallic environment than the outer In rows. These assertions support the results of ARPES by Yeom *et al.*[12] Once the surface structure has been transformed from (4×1) to (8×2), the *p*-state charges within Wigner Seitz radius, 1.312 Å, of the Si adatoms do not change. However, the *p*-state charges within Wigner Seitz radius 1.677 Å, of the outer In adatoms change from 0.803*e* per adatom in the (4×1) to 0.900*e* and 0.908*e* [for In(1) and In(2), respectively] in the (8×2) phase. The *p*-state charges per inner In adatom, In(3), In(4), In(5), and In(6) vary from 1.006*e*, 1.006*e*, 1.021*e*, and 1.021*e* to 0.927*e*, 1.055*e*, 1.067*e*, and 0.944*e*, respectively. Although the difference between each values for the (4×1) and the (8×2) phases are still small, one starts to find changes in the change of atomic structure. Therefore, we can say that during phase changes, surface adatom reconstruction also redistributes the electric charges and forms charge-density wave.

There has been a long-standing controversy whether the phase transition of In adsorbed on the Si(111) surfaces can be considered as a CDW transition or not. We will simply review the mechanics of CDW formation in a one-dimensional system.[30] Suppose that there is a static distortion with wave vector *q*. The lattice distortion increases the strain energy of the system and also induces a potential for electrons. The electron-phonon coupling triggers charge redistribution. A bandgap is then introduced to decrease the kinetic energy of the electron system. From the band theory we know that an energy band has a gap at the Brillouin zone boundary. Hence, in the CDW state, both the lattice of the ion and the electron charge density are spatially modulated with the same wave vector $q=2k_F$. A stabilized CDW state is formed if the electronic energy gain due to the gap formation overcomes the loss in elastic energy. We have confirmed that the atomic reconstruction induces the formation of CDW and that the existence of pseudogaps lowers the total system's energy during the phase changes from the (4×1) to the (8×2). Therefore, the controversy seems to be cleared up, although some issues are still left unsolved (such as the role of *d* electrons). The transition temperature has not been decided yet experimentally to our knowledge. However, the theoretical transition temperature T_C^{MF} can be decided according to the mean-field approximation $2\Delta=3.52k_BT_C^{\mathrm{MF}}$ for a one dimension weak coupling CDW system.[30] The transition temperature T_C^{MF} can be estimated to be 102 K which is close to the observed temperatures of the (8×2) phase by the reported experiments, 70,[11] 100,[8] or 130 K.[13] Hence, this system can be considered as a weakly coupled one-dimensional electron-lattice system.

In summary, the atomic and electronic structures of In overlayers on an Si(111) surface were calculated from first principles according to the density-functional theory. The atomic structures of the (4×1)- and (8×2)-In/Si(111) surfaces that were determined, are very much consistent with the experimental data obtained by Bunk *et al.*[2] and by Kumpf *et al.*,[14] respectively. Our calculated atomic structure model of the (4×1) phase was also consistent with other theoretical calculations,[15–17] while, to our knowledge, no other theoretical calculation has as yet reported the experimental observed (8×2) structure. In the (4×1) phase, the In chains are found to exhibit quasi-one-dimensional metallic behavior, with three surface-state bands' crossing the Fermi level in the $\overline{\Gamma X}_1$ direction (parallel to the In chains). The calculated band structure is in excellent agreement with the ARPES results[7,8,12] and is consistent with the other theoretical calculation.[16] From the partial density of state, it seems that the inner rows of the In chains are more metallic than the outer rows as suggested by Yeom *et al.*[12] As the surface structure is transformed from the (4×1) phase to the (8×2) phase, the pairing of the outer In adatoms in the In chains, and the opposite directions of the displacements of the Si atoms in the neighboring Si rows are consistent with the results from x-ray diffraction. For the (4×2) phase, it is shown that the pairing effect doubles the periodicity along the chain and lowers the total system's energy. When the structure phase changes to the (8×2) phase, the pairing of outer In atoms becomes stronger, and the displacements in the opposite directions of the neighboring Si zigzag chains generate a glide symmetry. Atomic reconstruction also redistributes the valence electron charge, rearranges the electronic bands, splits the bands, opens up small pseudogaps at the surface Brillouin zone boundary (at points $\overline{X}_2$ and $\overline{Y}$). These phenomena are characteristic of the formation of the CDW state in a quasi-one-dimensional system. Hence, we believe the phase transition between the (4×1) and (8×2) phases on the Si(111) surface is driven by a charge-density wave. The shorter interchain distance and the valence charge density distribution also reveal significant interchain interaction between adjacent In chains in the (8×2) phase. The valence charge density distribution of the (8×2) phase is also compatible with the STM images at low temperatures. Our results are consistent both with the structural model for the low-temperature phase and with the idea of a fluctuating one-dimensional charge-density wave state.

The author would like to thank the National Science Council of the Republic of China, Taiwan for financially supporting this research under Contract Nos. NSC 91-2112-M-110-011 and 92-2112-M-110-006. Dr. Wu-Pei Su, Dr. Ching Cheng, and Dr. Ching-Ming Wei are appreciated for their helpful discussions. Computing resources were provided by the National Center for High-performance Computing.

*Email address: tsaysf@mail.nsysu.edu.tw

[1] J. J. Lander and J. Morrison, J. Appl. Phys. **36**, 1706 (1965).
[2] O. Bunk, G. Falkenberg, J. H. Zeysing, L. Lottermoser, R. L. Johnson, M. Nielsen, F. Berg-Rasmussen, J. Baker, and R. Feidenhans'l, Phys. Rev. B **59**, 12 228 (1999).
[3] J. Kraft, M. G. Ramsey, and F. P. Netzer, Phys. Rev. B **55**, 5384 (1997).
[4] J. L. Stevens, M. S. Worthington, and I. S. T. Tsong, Phys. Rev. B **47**, 1453 (1993).
[5] A. A. Saranin, A. V. Zotov, K. V. Ignativoch, V. G. Lifshits, T. Numata, O. Kubo, H. Tani, M. Katayama, and K. Oura, Phys. Rev. B **56**, 1017 (1997).
[6] A. A. Saranin, A. V. Zotov, V. G. Lifshits, J.-T. Ryu, O. Kubo, H. Tani, T. Harada, M. Katayama, and K. Oura, Phys. Rev. B **60**, 14 372 (1999).
[7] T. Abukawa, M. Sasaki, F. Hisamatsu, T. Goto, T. Kinoshita, A. Kakizaki, and S. Kono, Surf. Sci. **325**, 33 (1995).
[8] H. W. Yeom, S. Takeda, E. Rotenberg, I. Matsuda, K. Horikoshi, J. Schaefer, C. M. Lee, S. D. Kevan, T. Ohta, T. Nagao, and S. Hasegawa, Phys. Rev. Lett. **82**, 4898 (1999).
[9] I. G. Hill and A. B. McLean, Phys. Rev. B **56**, 15 725 (1997); **59**, 9791 (1999); Phys. Rev. Lett. **82**, 2155 (1999).
[10] S. Mizuno, Y. O. Mizuno, and H. Tochihara, Phys. Rev. B **67**, 195410 (2003).
[11] S. V. Ryjkov, T. Nagao, V. G. Lifshits, and S. Hasegawa, Surf. Sci. **488**, 15 (2001).
[12] H. W. Yeom, K. Horikoshi, H. M. Zhang, K. Ono, and R. I. G. Uhrberg, Phys. Rev. B **65**, 241307 (2002).
[13] K. Sakamoto, H. Ashima, H. W. Yeom, and W. Uchida, Phys. Rev. B **62**, 9923 (2000).
[14] C. Kumpf, O. Bunk, J. H. Zeysing, Y. Su, M. Nielsen, R. L. Johnson, R. Feidenhans'l, and K. Bechgaard, Phys. Rev. Lett. **85**, 4916 (2000).
[15] J-H Cho, D-H Oh, K. S. Kim, and L. Kleinman, Phys. Rev. B **64**, 235302 (2001).
[16] J. Nakamura, S. Watanabe, and M. Aono, Phys. Rev. B **63**, 193307 (2001).
[17] R. H. Miwa and G. P. Srivastava, Surf. Sci. **473**, 123 (2001).
[18] G. Kresse and J. Hafner, Phys. Rev. B **47**, 558 (1993); **49**, 14 251 (1994).
[19] G. Kresse and J. Furthmüller, Comput. Mater. Sci. **6**, 15 (1996).
[20] G. Kresse and J. Furthmüller, Phys. Rev. B **54**, 11 169 (1996).
[21] D. M. Ceperley and B. J. Alder, Phys. Rev. Lett. **45**, 566 (1980).
[22] J. P. Perdew and A. Zunger, Phys. Rev. B **23**, 5048 (1981).
[23] P. E. Blöchl, Phys. Rev. B **50**, 17953 (1994); G. Kresse and D. Joubert, *ibid.* **59**, 1758 (1999).
[24] H. J. Monkhorst and J. D. Pack, Phys. Rev. B **13**, 5188 (1976).
[25] For example, the max deviation given by Nakamura *et al.* (Ref. 16) based on DFT in the generalized gradient approximation (GGA) is 0.16 Å, and the max deviation along the [111] direction given by Miwa *et al.* (Ref. 17) based on DFT in the LDA is 0.13 Å.
[26] Shiow-Fon Tsay and M.-H Tsai (private communication).
[27] *Table of Periodic Properties of the Elements* (Sargent-Welch, Illinois, 1980).
[28] We believe our calculations are sufficiently accurate to distinguish energy difference between different structures of 1 meV per (8×2) unit cell. The (8×2) structure also was obtained using the other computational approach (Ref. 26).
[29] L. J. Sham and M. Schlüter, Phys. Rev. Lett. **51**, 1888 (1983). The LDA has been demonstrated to be sufficiently accurate in determining the ground-state characteristics of metals and semiconductors; however, when the eigenvalues of the Kohn-Sham equation are regarded as the single-particle excitation energies, the reliability varies. Accordingly, the LDA is satisfactory for metals, but the errors in the semiconducting band gaps can be as high as 50%.
[30] T. Aruga, J. Phys.: Condens. Matter **14**, 8393 (2002); G. Grünner, *Density Waves in Solids* (Addison-Wesley, Reading, MA, 1994).